

Adaptation of antenna profiles for control of MR guided hyperthermia (HT) in a hybrid MR-HT system

Mirko Weihrauch¹, Peter Wust¹, Martin Weiser²,
Jacek Nadobny¹, Steffen Eisenhardt¹,
Volker Budach¹, Johanna Gellermann¹

¹ Clinic for Radiation Oncology
Charité – Universitätsmedizin Berlin
Campus Virchow Klinikum
Augustenburger Platz 1, 13353 Berlin, Germany

² Zuse Institute Berlin
Department Numerical Analysis and Modelling
Takustr. 7, 14195 Berlin, Germany

(Received 15 May 2007; accepted for publication 2 October 2007
in *Medical Physics*)

Key words: hyperthermia, MRI, closed-loop control, antenna profiles, FDTD, Gauss-Newton algorithm

Abstract

A combined numerical-experimental iterative procedure, based on the Gauss-Newton algorithm, has been developed for control of magnetic resonance (MR) - guided hyperthermia (HT) applications in a hybrid MR-HT system BSD 2000 3D-MRI. In this MR-HT system, composed of a 3-D HT applicator Sigma-Eye placed inside a tunnel-type MR tomograph Siemens MAGNETOM Symphony (1.5 T), the temperature rise due to the HT radiation can be measured on-line in three dimensions by use of the proton resonance frequency shift (PRFS) method. The basic idea of our iterative procedure is the improvement of the system's characterization by a step by step modification of the

theoretical HT antenna profiles (electric fields radiated by single antennas). The adaptation of antenna profiles is efficient if the initial estimates are radiation fields calculated from a good a priori electromagnetic model. Throughout the iterative procedure, the calculated antenna fields (FDTD) are step by step modified by comparing the calculated and experimental data, the latter obtained using the PRFS method. The procedure has been experimentally tested on homogeneous and inhomogeneous phantoms. We show that only few comparison steps are necessary for obtaining a dramatic improvement of the general predictability and quality of the specific absorption rate (SAR) inside the MR-HT hybrid system.

I. Introduction

Regional hyperthermia, performed with phase steered ring applicators like the Sigma-60 applicator, has been in use since 15-20 years. With this technique different groups world wide have derived extraordinary clinical results in combined therapies with radiation therapy, chemotherapy, and radiochemotherapy.^{1,2,3} Also the relationship of higher temperatures with improved clinical results has been shown,^{4,5} see also Wust et al.⁶ for an overview.

Earlier, model calculations have displayed that navigation and resulting temperature distributions are improved by better applicator design.^{7,8,9,10} The overall strategy was to increase the number of antennas, resulting in an improved navigation of the power distribution. Applicators according to this design have been constructed and are in clinical use since a few years (Sigma-Eye applicator with 12 channels compared to four channels in Sigma-60).

The main task in designing a therapy is to come up with an applicator control consisting of amplitude and phase delay for each antenna that leads to an individually optimal temperature distribution inside the patient. There are two essentially different strategies to accomplish this: (a) using physical and physiological models of the applicator and patient, respectively, to compute the electrical fields, energy absorption, and temperature distribution, followed by an a priori optimization of the applicator control, and (b) using a feedback control loop to drive the applicator towards the optimal adjustment during the therapy.

Strategy (a) involves solving the time-harmonic Maxwell's equations by FDTD (finite-difference time-domain^{11,12,13}) or FE (finite element^{8,10,14}) methods, as well as the bio-heat-transfer equation.¹⁵ Multiple models and planning systems have been developed in the last decades^{16,17,18} and have been evaluated in phantoms.^{19,20,21} In principle, these computations can be performed with relatively high accuracy in acceptable time (45 *min* on PC: AMD, 2.2 Ghz). For example, a combined electromagnetic-thermal comparison between simulations on 1cm voxel grids and measured 3-D MR-temperature data sets in patients resulted in an average temperature deviation of 0.45°C which corresponds to a relative deviation of around 18%.²⁰ However, inevitable modeling errors in the phantom/patient geometry and tissue behavior, variations in the feeding network, and inaccurate amplifier behavior often lead to inexact results.

Strategy (b) circumvents the need for a correct physical model by directly controlling the temperature during the therapy. In most cases, one or more temperature measurements are necessary for controlling the temperatures, usually achieved by power changes of one or more channels. Here the characteristics and stability of the controller, e. g. reaction to disturbances are important to consider.^{22,23}

In the hyperthermia related literature some control loops have already been described. If a linear time dependent model $y(t) = -Ku(t)$ mapping the control settings u to the state variables y is assumed, and a quadratic quality functional $J(y)$ is to be minimized, the controller output satisfies a certain matrix equation (so-called Riccati equation).²⁴ Due to its increasing computational complexity, this method is limited to low-dimensional systems with few control settings and state variables.

The application of such a feedback controller has been mainly focused on the navigation of ultrasound HT applicators. Hutchinson et al.²⁴ proposed a controller based on an increase of temperatures (in n measurements) depending on m power levels (of ultrasound transducers). Arora et al.²⁵ presented a formulation for an optimal control, using the descriptors of thermal dosimetry (T90 and thermal dose) by applying a linear approximation of a highly nonlinear problem. The introduction of thermal dose (which continues to accumulate even after power is turned off) required the development of a model predictive controller. In both cited articles, the control plans were applied only for simulated thermal therapies, examining the influences of measurement errors, noise, and imprecision of the model.

At the Charité, a hybrid MR-HT system integrating a Sigma-Eye applicator and an 1.5T MR scanner has been established.²⁶ This hybrid system allows non-invasive MR-measurements of 3D temperature distributions inside phantoms and patients,²⁷ and therefore provides the prerequisites to conduct MR-guided regional hyperthermia in a closed control loop.

A transfer of the aforementioned algorithms to MR-guided HT is impractical due to the high number of spatial temperature measurements (state variables y) to be respected. A different control scheme based on MRI monitoring has been introduced by Kowalski et al.^{28,29} for hyperthermia and applied to a phantom in a quasi 2D applicator with one antenna ring. Their method is based on the representation of the specific absorption rate (SAR) in the form

$$\text{SAR} = u^H M u, \quad (1)$$

where u is the complex control vector and M a hermitian action matrix (see also Das et al.³⁰ and Köhler et al.³¹). In a set-up phase, M is identified from MR measurements of many, sufficiently exciting control vectors. Afterwards, (1) can be used directly to optimize any SAR-dependent quality functional.

With modern applicators with $n = 12$ independent channels, such as the Sigma-Eye applicator, and more so for actual therapy, the approach based on complete identification of M has a severe drawback. For an applicator with n independent channels, M contains n^2 degrees of freedom, such that at least n^2 measurements are required for a full identification. For probably this reason, the simulations in Kowalski et al.^{28,29} were restricted to a six-channel applicator and the phantom experiments limited to only three

channels. Note that for the Sigma-Eye applicator 144 measurements would be necessary. In a clinical therapy, the required set-up phase would last several hours even the actual treatment could start. Moreover, the control settings for which the measurements are taken have to span the whole control space (called “sufficiently exciting” in Kowalski et al.^{28,29}). Applied to actual hyperthermia treatments, this means that the patient would have to endure a lot of clinically suboptimal SAR distributions, probably provoking unfavorable physiological counter-regulations.

We are thus facing the challenge to devise a controller that delivers a near-optimal therapy using much fewer measurements than are necessary to perform a full model identification. We therefore propose a different approach combining strategies (a) and (b) mentioned above. Starting with the available, physically well-founded, though only approximative numerical a priori models, we adapt them, taking relatively few measurements into account. Such an adaptation scheme is described in the following section. The experimental results given in Section D suggest that this combination of approaches (a) and (b) is quite promising.

II. Methods

In this section we describe the control scheme. It differs from Kowalski et al.²⁸ in two aspects: a priori knowledge from planning computations is taken into account, and the identification is geared towards the antenna profiles instead of the action matrix. Before such an online control with integrated optimization can be applied to hyperthermia treatment of patients, it is necessary to validate the method at phantoms. This validation is to be investigated in the following.

A. Mathematical model

The total electrical field E of a hyperthermia applicator with n antennas can be described by a linear combination of the antenna profiles V^ν , $\nu = 1, \dots, n$ radiated by the single antennas:

$$E = \sum_{\nu=1}^n u^\nu V^\nu = Vu \quad (2)$$

where $u^\nu \in \mathbb{C}$ are the complex control settings associated with the amplifier channels.

From the electric field, the SAR can be computed as

$$\text{SAR} = \frac{\sigma}{2}|E|^2 = \frac{\sigma}{2}u^H V^H V u. \quad (3)$$

The superscript H denotes the complex conjugate transpose. Note that the action matrix can be recovered as $M = V^H V$.

The evolution of the temperature distribution inside an unperfused phantom during hyperthermia is described by the time-dependent bio heat transfer equation

$$\text{div}(\kappa \nabla T) + \rho \cdot \text{SAR} = \rho c \frac{\partial T}{\partial t}, \quad (4)$$

where T is temperature (K), t is time (s), SAR is specific absorption rate (W/kg), κ is thermal conductivity ($W m^{-1}K^{-1}$), ρ is density (kg/m^3), and c is heat capacity ($Ws kg^{-1}K^{-1}$). Neglecting thermal diffusion, which is admissible for small κ or smooth temperature distributions, and small time differences Δt , the SAR can be approximated by SAR^M obtained from temperature measurements T^M as SAR^M .

$$SAR \approx SAR^M = c \frac{\Delta T^M}{\Delta t} \quad (5)$$

For further details see Wust et al.,³² Tilly et al.³³

B. Procedure to adapt the antenna profiles of a hyperthermia applicator

As mentioned in the introduction, we assume that the initial antenna profiles V_0 obtained from an a priori simulation are a reasonable approximation to the antenna profiles V . Given k measurements to arbitrary control settings u_i , $i = 1, \dots, k$, either V_0 or $M_0 = V_0^H V_0$ can be adapted to V_k or M_k respectively such that the computed values

$$SAR_i = \frac{\sigma}{2} u_i^H V_k^H V_k u_i = \frac{\sigma}{2} u_i^H M_k u_i \quad (6)$$

match the measured data SAR_i^M as closely as possible. Since V consists of n complex-valued vectorial E-fields, the number of real degrees of freedom in V is $n * 2 * 3 = 6n$ compared to n^2 real degrees of freedom in the complex hermitian matrix M . Thus we feel that for $n > 6$ and $k \ll n^2$, the smaller model based on adaptation of V_0 is more appropriate than adaptation of M_0 . We therefore aim at minimizing

$$g(V) = \|F(V)\|^2, \quad (7)$$

with

$$F(V) = \begin{pmatrix} \frac{\sigma}{2} u_1^H V^H V u_1 - c \frac{\Delta T_1}{\Delta t_1} \\ \vdots \\ \frac{\sigma}{2} u_k^H V^H V u_k - c \frac{\Delta T_k}{\Delta t_k} \end{pmatrix}. \quad (8)$$

F represents the mismatch between measurements and model prediction. For solving (7), the Gauss-Newton method (see e. g. Deuffhard et al.³⁴)

$$\begin{aligned} \Delta V^j &= -F'(V^j)^+ F(V^j) \\ V^{j+1} &= V^j + \Delta V^j, \quad j = 0, \dots \end{aligned} \quad (9)$$

is applied, where $F'(V^j)^+$ denotes the pseudoinverse of $F'(V^j)$. The iteration (9) is terminated as soon as $\|\Delta V^{j^*}\| \leq \varepsilon$ for some j^* , and we set $V_k = V^{j^*}$. In our computations we have chosen $\varepsilon = 10^{-5}$. Note that F is not complex differentiable, such that a realification of F has to be used.

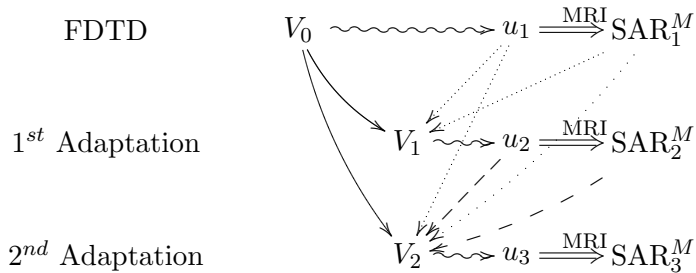


Figure 1: Successive adaptation of the antenna profiles V . The control settings u can be determined based on the optimization of a quality functional as measurements become available (closed-loop control). MRI denotes the MR-measurement for the determination of the SAR. Arrows indicate the input data record for each respective calculation. The double arrow (\Rightarrow) stands for the measurement and the sidled arrow (\rightsquigarrow) means selection of control settings u_i

For few measurements, the least squares problem (7) is highly underdetermined, such that infinitely many solutions exist. Since V_0 is assumed to be a physically well-founded approximate solution, it is desirable to choose a solution V_k with minimal distance to V_0 . This is realized by application of the pseudoinverse $F'(V^j)^+$ in each Gauss-Newton step. In passing we note that a good initial value V_0 results in a fast local convergence of the Gauss-Newton method.

This leaves the question how to choose the control settings u_i . In principle, any set of sufficiently different control settings can be used for adaptation of the antenna profiles. However, since during actual hyperthermia one will aim at treating the patient with the best therapy currently known, the control settings u_i should rather be computed by optimizing a given quality functional using the best available model V_{i-1} , sequentially as measurements become available (closed-loop control). This procedure is illustrated in Figure 1.

III. Experiments

The practical benefit that can be obtained by adaptation of antenna profiles as described in Section II has been evaluated in a series of heating experiments using two different phantoms.

A. Experimental set-up

The heating experiments were performed in two different phantoms (homogeneous and heterogeneous) centered in the SIGMA-Eye HT applicator (BSD Corp., Salt Lake City, Utah, USA) with a size of 40 x 58 x 50 cm. The homogeneous phantom has a shape of a circular cylinder of 30 cm diameter and 40 cm length. It is filled with a

so-called “superstuff” ($\sigma = 0.55 \text{ S/m}$, $\epsilon_r = 78$, equivalent to so-called “2/3 medium”). The heterogeneous phantom has a shape of an elliptical cylinder of $21 \times 35 \times 50 \text{ cm}$ with a skeleton embedded into a tissue-like agarose (2/3 medium, see above). For further details see Gellermann et al.¹⁹

The power deposition patterns in the phantoms can be controlled by adjusting the phases and the amplitudes of the 12 channels of the HT applicator. The channels feed antennas are organized in three transversal antenna rings (Feet, Middle, Head). Control settings u_i are specified as phase delays in ventral, dorsal, right, and left channels in each ring. For a detailed description of the SIGMA-Eye applicator (especially with respect to the modeling of its feed networks) and experimental and numerical investigation of the relationship between its forward and feed point parameters (HT amplitudes and phases) see Nadobny et al.¹⁸ Details of modeling, measurements and proposed improvements can also be found in Wust et al.^{35,36}

The temperature (increment) distributions that were generated in the phantoms during the heating intervals were acquired three-dimensionally by means of MR-thermography. The applicator was inserted into the bore of a 1.5 Tesla MR-tomograph (Magnetom Symphony, Siemens, Erlangen, Germany) using a special rail system as described in Gellermann et al.²¹ Technical details describing an operation of the HT applicator under simultaneous MR-monitoring have been presented previously.^{19,37}

A summary of available MR-thermography methods is outlined in Gellermann et al.²⁷ The experiments were based on the proton resonance frequency shift method (PRFS),³⁸ which had been shown to provide the most accurate temperature information. In all experiments a spoiled echo gradient sequence with $\text{TR} = 750 \text{ ms}$ and two echo times $\text{TE} = 4 \text{ ms}$ and 20 ms , flip angle 50° was used. 40 slices (1 cm slice thickness without gap) with a matrix size of 128×128 and a field of view (FOV) of 50 cm were acquired. The total acquisition time was 2 min .

Uncorrected MR phase datasets were acquired with the user software of the MR-scanner (Siemens SYNGO). These datasets were post-processed in a planning station using AMIRA-HyperPlan³⁹ in order to calculate and to visualize the drift-corrected MR-temperature (increment) distributions.^{36,40} The post-processing procedure needs about 10 s . These methods were validated^{19,20} with a temperature error below $0.5 \text{ }^\circ\text{C}$. This accuracy was verified selectively using 4 temperature probes placed in catheters and comparing these direct measurements with MR-temperatures. Further details can be found in Gellermann et al.^{5,21}

A three-dimensional SAR dataset of $128 \times 128 \times 40$ voxels of dimensions $0.39 \times 0.39 \times 1 \text{ cm}$ each was registered in the tissue-equivalent portion of two phantoms. No measurable MR signal was received in the skeletal part of the heterogeneous phantom.

B. Test procedure

The procedure was analyzed in 17 test series. Four of them were performed with the homogeneous phantom, and 13 with the inhomogeneous phantom. First, the initial antenna profiles V_0 were computed using the FDTD method on a cartesian grid with

cells of dimension $1 \times 1 \times 1 \text{ cm}$. Special care has been taken to compute the FDTD on the exact geometry given by the actual relative positioning of phantom and HT applicator inside the MR bore. The antenna profiles were then linearly interpolated onto the voxel grid used for obtaining the MR-measurements (see formula A1, A2 in Appendix from Nadobny et al.⁴¹). Then, during each test series, four different control settings were applied sequentially. For each control setting a reference data set was acquired before heating. After heating with 900 W for $\Delta t = 5 \text{ min}$, the acquisition of another MR-dataset (acquisition time $\approx 2 \text{ min}$) starts, with still power on (Table 1). Note that Δt must be clearly longer than the temperature acquisition time ($\approx 123 \text{ s}$) during the MR-sequence in order to suppress intra acquisitional smoothing effects. The choice of the particular heating time interval $\Delta t \approx 5 \text{ min}$ as used in this paper is explained in Nadobny et al.²⁰(Section IVB2iii). Furthermore from our long-term MR-measurement experience we notice that the applied power of 900 W guarantees an average temperature rise of around 3°C during the aforementioned heating time interval, which is a value clearly higher than the general MR-measurement accuracy of around 0.5°C . From the temperature difference of both datasets, a measurement SAR^M is computed according to (5).

After each SAR-measurement, the power was switched off for an appropriate time ($\approx 5 \text{ min}$) until a quasi-stationary state had been reached (see **B. Design of the experiments** in Gellermann et al.²¹). For most test series, the next control setting was determined by simultaneously maximizing the SAR in some region of interest and minimizing the SAR outside this region on base of the adapted antenna profiles (see Fig. 1 and Table 1). On the other hand complementary control settings were adjusted in test series, e.g. 5 cm left, 5 cm right, 5 cm ventral, 5 cm dorsal in the axial plane. Because the aim of this investigation is to examine the adaptation procedure. After the equilibration period, the measurement cycle for the next control settings was started (Table 1). The duration of one measurement cycle amounts to 14 min. The adaptation of the antenna profiles can be calculated after the whole test procedure, if the control settings were determined before the measurements start (Table 1).

C. Comparison of measurement and planning

It is important to note that the least-squares approach (7)–(9) is independent of any ordering of the measurements in one test series, even if the control settings were obtained by successive optimization. Moreover, arbitrary subsets of test series can be used in a retrospective analysis for assessing the possible benefit of the presented approach for correctly predicting SAR distributions.

Since (7) is underdetermined, exact reproduction of SAR distributions for control settings u_i can be expected when the corresponding measurement SAR_{*i*}^M is included in the set used for adapting the antenna profiles. This trivial case is of course not the aim of our comparison. We are investigating the improvement of predictability. Therefore, in the results presented below, the measurement to which the computed SAR is compared is never included in the set of measurements used to adapt the antenna profiles. An

	step	time	action
preparation	I	-51 <i>min</i>	positioning phantom in the BSD-System in the MR-scanner
	II	-49 <i>min</i>	MR-measurement
	III	-45 <i>min</i>	starting calculation of FDTD antenna profiles based on the MR-measurement
measurement cycle 1	1	0 <i>min</i>	MR-thermometry measurement (reference dataset)
	2	2 <i>min</i>	Power on! 900 W, control setting u_1
	3	7 <i>min</i>	MR-thermometry measurement $\rightarrow \text{SAR}_1^M$
	4	9 <i>min</i>	Power off!
	5	9 <i>min</i>	SAR-calculation based on the two MR-thermometry measurements
in case of online control	6	12 <i>min</i>	adaptation of antenna profiles
	7	15 <i>min</i>	optimizing SAR in a target region (closed loop control) \rightarrow control setting u_2
measurement cycle 2	1	14 or 17 <i>min</i>	MR-thermometry measurement (reference dataset)
	\vdots	\vdots	\vdots

Table 1: Workflow of test procedure. Step 6 and 7 demonstrate the integration of the adaptation procedure in a closed control loop.

example for a possible comparison: The measured SAR_3^M in the third measurement cycle can be compared with the computed $\text{SAR}_I = \frac{\sigma}{2} u_3^H V_0^H V_0 u_3$ based on the standard antenna profiles V_0 and with the computed $\text{SAR}_{II} = \frac{\sigma}{2} u_3^H V_2^H V_2 u_3$ based on the adapted antenna profiles V_2 , which were adapted from the two measurement cycles before (see Fig. 1 and Tab. 1).

Deviations between measured and computed SAR distributions are quantified by the root mean square error

$$\Delta\text{SAR} = \sqrt{\frac{1}{N} \sum_{i=1}^N (\text{SAR}^M(v_i) - s\text{SAR}(v_i))^2},$$

where the computed SAR is normalized to yield the same total power as the measured SAR by

$$s = \frac{\sum_{i=1}^N \text{SAR}^M(v_i)}{\sum_{i=1}^N \text{SAR}(v_i)}.$$

Here, N is the number of voxels v_i for which reliable MR data was available. In particular, voxels in skeletal regions and close to tissue boundaries were excluded from comparison. For all test series, at least 60 000 voxels were used.

The adaptation of the antenna profiles based on the FDTD planning, as described in Figure 1, lasted around “ k minutes” (k : number of measurements) with a PC: P IV, 1.5 GHz.

D. Results

Deviations between measured and computed SAR distributions are shown in Table 2 for different numbers of measurements k used for adaptation of antenna profiles and both phantoms. The computed SAR based on the adapted antenna profiles ($k > 0$) is significantly more precise: In the homogeneous phantom, the error has been reduced by 30%, whereas in the heterogeneous phantom, the error reduction was even 50%.

Next, in Fig. 2-4 we show results based on antenna profile adaptations using arbitrary (but of course belonging to the same test series) control settings, while in Fig. 5 we present the closed-loop principle using sequentially optimized control settings as measurements become available (see Fig. 1).

Figure 2 shows a comparison between SAR distributions computed by original FDTD ($k = 0$) and the corresponding MR measurement for a certain control setting u_a in the heterogeneous phantom. The deviation ΔSAR is as high as 4.7 W/kg . Figure 3 presents the improvement of the SAR prediction by use of only one adaptation step ($k = 1$) in the heterogeneous phantom. Two predictions, one in Fig. 3a (for $k = 0$, FDTD), and another in Fig. 3b (for $k = 1$), are compared with the corresponding MR measurement shown in Fig. 3c. The comparison in Fig. 3 is performed for control setting u_b . Left, in Fig. 3a, the original FDTD prediction for u_b is shown. The deviation between Fig. 3a ($k = 0$, FDTD) and measurement in Fig. 3c is as high as $\Delta\text{SAR} = 4.0 \text{ W/kg}$. In Fig. 3b ($k = 1$), the improved prediction for u_b is displayed, using the adapted antenna profiles

k	n	homogeneous phantom		n	heterogeneous phantom	
		$\Delta\text{SAR} [W/kg]$	relative error		$\Delta\text{SAR} [W/kg]$	relative error
0	20	3.5 ± 0.8	1.0 ± 0.0	64	3.9 ± 0.8	1.0 ± 0.0
1	82	2.8 ± 1.0	0.8 ± 0.2	256	2.3 ± 0.8	0.6 ± 0.2
2	132	2.5 ± 0.9	0.7 ± 0.2	396	2.1 ± 0.7	0.5 ± 0.2
3	104	2.4 ± 0.7	0.7 ± 0.2	292	2.0 ± 0.7	0.5 ± 0.2
4	40	2.4 ± 0.6	0.7 ± 0.1	100	2.1 ± 0.7	0.5 ± 0.2

Table 2: Deviations between measured and computed SAR. k is the number of measurements used to adapt the antenna profiles. $k = 0$ corresponds to the FDTD. n is the number of predicted measurements, summed up over all test series.

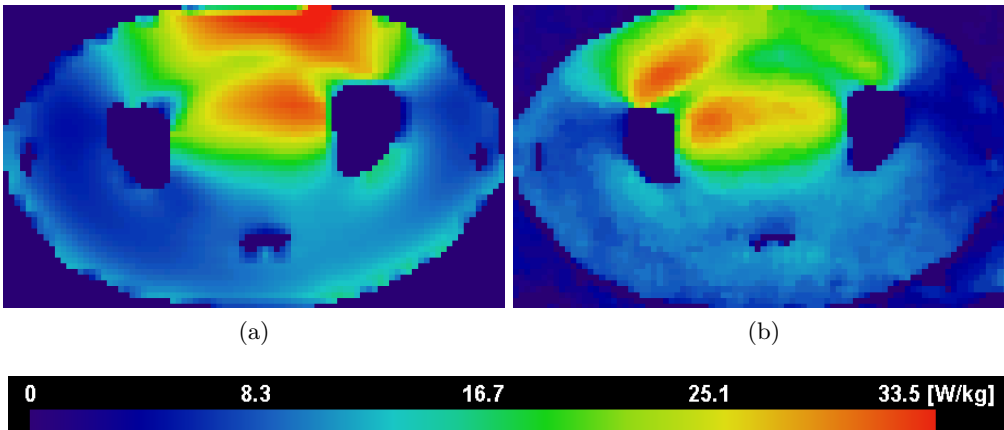


Figure 2: Comparison of FDTD ((a): $\text{SAR}(V_0, u_a)$) and measurement ((b): $\text{SAR}^M(u_a)$) in a transversal plane for the control setting $u_a = \{\text{Feet}(31,114,60,43)$ Middle(97,59,37,0) Head(56,43,32,44) $\}$. The deviation is $\Delta\text{SAR} = 4.7 W/kg$. Maximal measured SAR in the 3-D field of view (FOV): $53.2 W/kg$, averaged measured SAR in FOV: $14.8 W/kg$

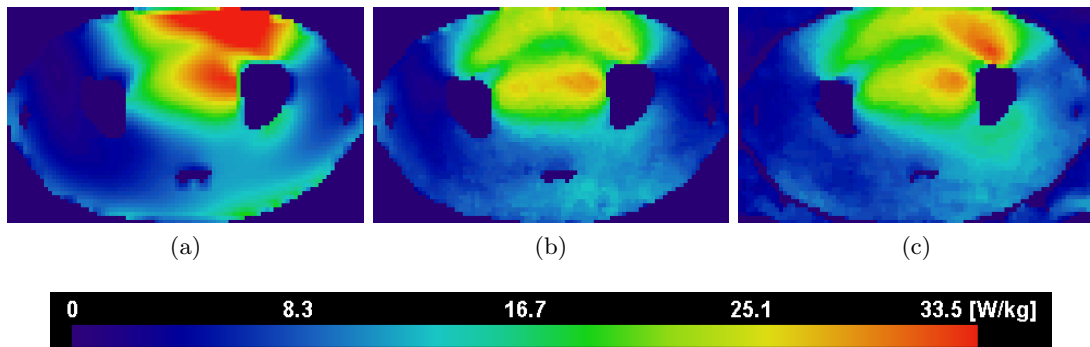


Figure 3: Improvement of SAR prediction for the control setting $u_b = \{\text{Feet}(40,139,82,69) \text{ Middle}(112,63,0,1) \text{ Head}(57,45,29,35)\}$ by adaptation of antenna profiles based on only one measurement for a *different* control setting u_a (in Fig. 2). (a): FDTD simulation for u_b : $\text{SAR}(V_0, u_b)$, (b): improved SAR prediction $\text{SAR}(V_1, u_b)$, (c): associated measurement $\text{SAR}^M(u_b)$.

Notice that (b) depends on the measurement $\text{SAR}^M(u_a)$ shown in Fig. 2b via the adapted antenna profiles V_1 computed by the Gauss-Newton algorithm. The deviation between (b) and (c) is reduced to $\Delta\text{SAR} = 2.6 \text{ W/kg}$ compared to the FDTD simulation of $\text{SAR}(V_0, u_b)$ in (a) with $\Delta\text{SAR} = 4.0 \text{ W/kg}$.

Maximal measured SAR in the FOV: 45.8 W/kg , averaged measured SAR in FOV: 14.2 W/kg

based on the measurement for the *different* control setting, u_a , previously shown in Fig. 2. The deviation ΔSAR has been reduced from 4.0 W/kg to 2.6 W/kg . Note that the control setting u_a used for adaptation differs significantly in several channels from the compared setting u_b : In homogeneous medium, the difference between u_a and u_b would lead to a focus shift of about 10 cm .

In Figure 4 a similar comparison as in Fig. 3 is carried out for control setting u_d , however for the homogeneous phantom. The deviation ΔSAR has been reduced from 3.4 W/kg to 1.8 W/kg . Again, a different setting u_c was used for adaptation. The difference between u_c and u_d leads to a focus shift of about $2\text{-}3\text{cm}$ (measurement for u_c not shown).

Finally, Fig. 5 shows the application of the antenna profile adaptation to the closed loop control introduced in Fig 1. In contrast to the situation in Fig. 3 and 4, the control settings have been obtained by simultaneous maximization of the SAR delivered to some target region and minimization of SAR outside this region (Table 1, step 6 and 7). Note that the quick convergence of the optimized control settings leads to small differences between the control settings used for adaptation and prediction, respectively, resulting in a better error reduction and simultaneously an improved heating of the target region.

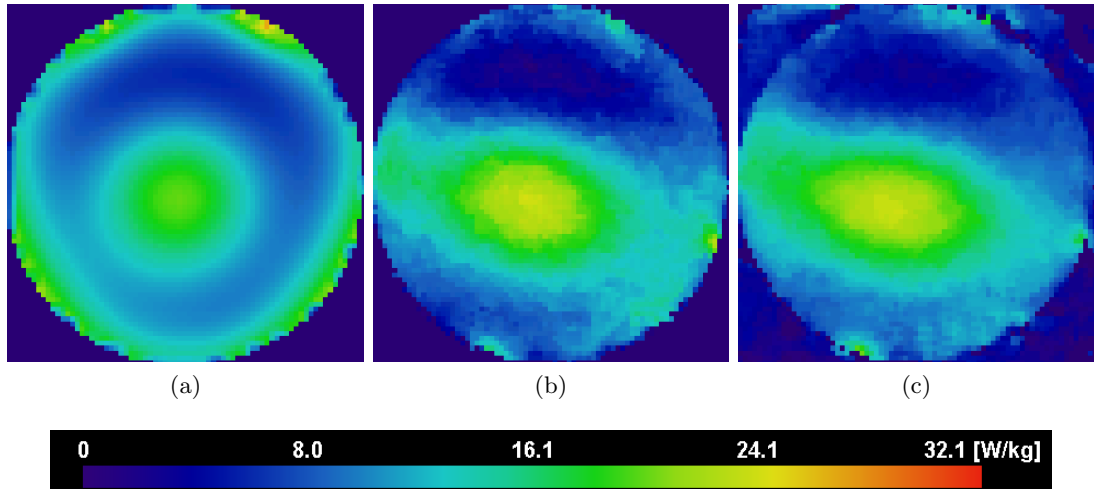


Figure 4: Improvement of SAR prediction in the homogeneous phantom for the control setting $u_d = \{\text{Feet}(21,26,34,14) \text{ Middle}(24,9,7,327) \text{ Head}(7,12,0,10)\}$ by adaptation of antenna profiles based on only one measurement for a *different* control setting $u_c = \{\text{Feet}(21,41,34,28) \text{ Middle}(24,24,7,341) \text{ Head}(7,27,0,24)\}$. (a): FDTD simulation for u_d : $\text{SAR}(V_0, u_d)$, (b): improved SAR prediction $\text{SAR}(V_1, u_d)$, (c): associated measurement $\text{SAR}^M(u_d)$. The deviation between (b) and (c) is reduced to $\Delta\text{SAR} = 1.8 \text{ W/kg}$ compared to the FDTD simulation (a) $\text{SAR}(V_0, u_d)$ with $\Delta\text{SAR} = 3.4 \text{ W/kg}$. Maximal measured SAR in the FOV: 24.3 W/kg , averaged measured SAR in FOV: 11.4 W/kg

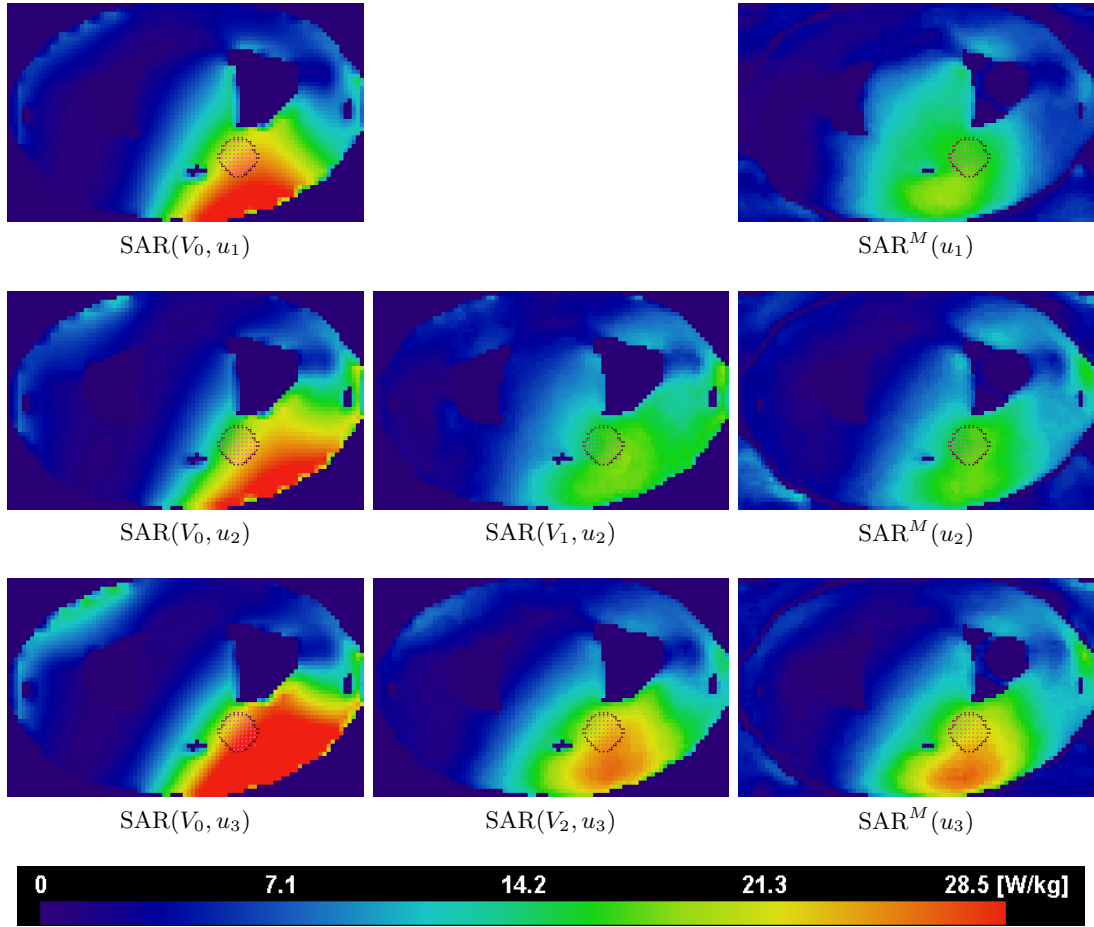


Figure 5: Proof of concept for closed loop control based on adaptation of antenna profiles according to Fig. 1.

Left column: FDTD without adaptation ($SAR(V_0, u_i)$).

Middle column: SAR computed using adapted antenna profiles ($SAR(V_{i-1}, u_i)$) with improved agreement with measurements.

Right column: SAR measurement ($SAR^M(u_i)$) with improved SAR exposition of the target region (dotted circle).

Rows 1, 2, 3: SAR distribution for control settings u_1, u_2, u_3 determined by successive maximization of SAR in the target region according to Fig. 1

IV. Discussion

It has been shown that the adaptation of antenna profiles with a Gauss-Newton method based on few MR thermometry measurements can improve the prediction and the quality of SAR distributions significantly in several experimental settings. Error reductions of up to 50% compared to a priori simulations with the FDTD method have been observed. The most important effect of the improved accuracy is, that therapy planning based on the adapted antenna profiles will lead to quite different optimal controls and deliver significantly more heat to the target region.

Given that the least squares approach is highly underdetermined ($6N = 72$ degrees of freedom in the model to be fitted versus no more than five measurements) such that a complete identification of the model is impossible, this result is positively surprising. We suppose that the good initial model supplied by the FDTD simulation is of vital importance for the successful application of least-squares fitting.

Particularly remarkable is that most of the error reduction (70% – 80%) is already achieved by adaptation based on the very first measurement. This fact can either be interpreted as an extraordinary success of the first adaptation step, or as a relative failure of subsequent adaptation steps. The first case would suggest the existence of an easily detectable, low-dimensional dominant error mode. In the second case, measurement errors such as noise or linearization error due to neglecting heat conduction, or possibly temperature-dependent material parameters, are likely reasons for the limited progress achieved by subsequent adaptation steps. It is not yet clear which case applies.

A less pronounced but clearly visible outcome is that the error reduction is better in the heterogeneous phantom than in the homogeneous one. This can be attributed to the greater challenge that a complex heterogeneous geometry poses to an a-priori simulation. On the other side the measured SAR-distribution in the heterogeneous phantom is more characteristic and pronounced (compare Fig. 3 and Fig. 4). In particular, positioning errors lead to larger deviations of the antenna profiles than in the homogeneous case — leaving more room for improvement by adaptation based on actual measurements.

The applicability of the adaptation to closed loop control has been demonstrated on phantoms, also under difficult conditions: adaptation on base of complementary control settings. Both the significant improvement already after one step and the better improvement in the heterogeneous phantom suggest that this approach is a first important step to online control of hyperthermia treatment of patients. For clinical applicability, additional problems have to be addressed, such as varying perfusion and patient movements. Control settings will be restricted to be therapeutically useful, and cannot be expected to span the whole control space. Moreover, the cooling-down times are unacceptable in a treatment situation and have to be avoided by taking heat conduction into account when computing SAR from temperature measurements. Furthermore the calculation of the initial Value V_0 (e. g. FDTD) before the start of the actual therapy, is not acceptable in clinical situation. The initial antenna profiles can be generated in a separate MR-session and shift to the actual patient position at begin of the therapy.

Acknowledgments

This work has been supported by grants of the Deutsche Forschungsgemeinschaft (DFG) (project WU 235/1-2) and the Berliner Sparkassenstiftung Medizin (project: “oxygenation in hyperthermia”). We gratefully thank for the support.

References

- ¹J. van der Zee, D. G. González, G. C. van Rhoon, J. D. van Dijk, W. L. van Putten, and A. A. Hart, “Comparison of radiotherapy alone with radiotherapy plus hyperthermia in locally advanced pelvic tumours: a prospective, randomised, multicentre trial. Dutch Deep Hyperthermia Group,” *Lancet* **355**(9210), 1119–1125 (2000).
- ²G. Sreenivasa, B. Hildebrandt, S. Kümmel, K. Jungnickel, C. H. Cho, W. Tilly, D. Böhrmer, V. Budach, R. Felix, and P. Wust, “Radiochemotherapy combined with regional pelvic hyperthermia induces high response and resectability rates in patients with nonresectable cervical cancer,” *Int. J. Radiat. Oncol. Biol. Phys.* **66**(4), 1159–1167 (2006).
- ³R. D. Issels, L. H. Lindner, P. Wust, P. Hohenberger, K. Jauch, S. Daugaard, U. Mansmann, W. Hiddemann, J. Blay, and J. Verweij, “Regional hyperthermia (RHT) improves response and survival when combined with systemic chemotherapy in the management of locally advanced, high grade soft tissue sarcomas (STS) of the extremities, the body wall and the abdomen: A phase III randomised prospective trial (EORTC-ESHO intergroup trial),” in *ASCO*, 2007.
- ⁴B. Rau, P. Wust, W. Tilly, J. Gellermann, C. Harder, H. Riess, V. Budach, R. Felix, and P. M. Schlag, “Preoperative radiochemotherapy in locally advanced or recurrent rectal cancer: regional radiofrequency hyperthermia correlates with clinical parameters,” *Int. J. Radiat. Oncol. Biol. Phys.* **48**(2), 381–391 (2000).
- ⁵J. Gellermann, B. Hildebrandt, R. Issels, H. Ganter, W. Wlodarczyk, V. Budach, R. Felix, P.-U. Tunn, P. Reichardt, and P. Wust, “Noninvasive magnetic resonance thermography of soft tissue sarcomas during regional hyperthermia: correlation with response and direct thermometry,” *Cancer* **107**(6), 1373–1382 (2006).
- ⁶P. Wust, C. H. Cho, B. Hildebrandt, and J. Gellermann, “Thermal monitoring: invasive, minimal-invasive and non-invasive approaches,” *Int. J. Hyperthermia* **22**(3), 255–262 (2006).
- ⁷P. Wust, M. Seebass, J. Nadobny, P. Deuffhard, G. Mönich, and R. Felix, “Simulation studies promote technological development of radiofrequency phased array hyperthermia,” *Int. J. Hyperthermia* **12**(4), 477–494 (1996).
- ⁸K. D. Paulsen, S. Geimer, J. Tang, and W. E. Boyse, “Optimization of pelvic heating rate distributions with electromagnetic phased arrays,” *Int. J. Hyperthermia* **15**(3), 157–186 (1999).
- ⁹H. Kroeze, J. B. V. de Kamer, A. A. D. Leeuw, and J. J. Lagendijk, “Regional hyperthermia applicator design using FDTD modelling,” *Phys. Med. Biol.* **46**(7), 1919–1935 (2001).
- ¹⁰M. Seebass, R. Beck, J. Gellermann, J. Nadobny, and P. Wust, “Electromagnetic phased arrays for regional hyperthermia: optimal frequency and antenna arrangement,” *Int. J. Hyperthermia* **17**(4), 321–336 (2001).
- ¹¹K. S. Yee, “Numerical solution of initial boundary value problems involving Maxwell’s equations in isotropic media,” *IEEE Trans. Antennas Propagat.* **17**, 585–589 (1966).

- ¹²D. M. Sullivan, O. P. Gandhi, and A. Taflove, “Use of the finite-difference time-domain method for calculating EM absorption in man models,” *IEEE Trans. Biomed. Eng.* **35**(3), 179–186 (1988).
- ¹³A. Taflove, *Computational Electrodynamics. The Finite-Difference Time-Domain Method*, Artech House, Boston, London, 1995.
- ¹⁴R. Beck, P. Deuffhard, R. Hiptmair, R. H. W. Hoppe, and B. Wohlmuth, “Adaptive multilevel methods for edge element discretizations of Maxwell’s equations,” *Surv. Math. Ind.* **8**, 271–312 (1999).
- ¹⁵H. H. Pennes, “Analysis of tissue and arterial blood temperatures in the resting human forearm. 1948,” *J. Appl. Physiol.* **85**(1), 5–34 (1998).
- ¹⁶B. J. James and D. M. Sullivan, “Direct use of CT scans for hyperthermia treatment planning,” *IEEE Trans. Biomed. Eng.* **39**(8), 845–851 (1992).
- ¹⁷J. B. V. de Kamer, H. Kroeze, A. A. D. Leeuw, and J. J. Lagendijk, “Quasistatic zooming of FDTD E-field computations: the impact of down-scaling techniques,” *Phys. Med. Biol.* **46**(5), 1539–1551 (2001).
- ¹⁸J. Nadobny, H. Föhling, M. J. Hagmann, P. F. Turner, W. Wlodarczyk, J. M. Gellermann, P. Deuffhard, and P. Wust, “Experimental and numerical investigation of feed-point parameters in a 3-D hyperthermia applicator using different FDTD models of feed networks,” *IEEE Trans. Biomed. Eng.* **49**(11), 1348–1359 (2002).
- ¹⁹J. Gellermann, W. Wlodarczyk, H. Ganter, J. Nadobny, H. Föhling, M. Seebass, R. Felix, and P. Wust, “A practical approach to thermography in a hyperthermia/magnetic resonance hybrid system: validation in a heterogeneous phantom,” *Int. J. Radiat. Oncol. Biol. Phys.* **61**(1), 267–277 (2005).
- ²⁰J. Nadobny, W. Wlodarczyk, L. Westhoff, J. Gellermann, R. Felix, and P. Wust, “A clinical water-coated antenna applicator for MR-controlled deep-body hyperthermia: a comparison of calculated and measured 3-D temperature data sets,” *IEEE Trans. Biomed. Eng.* **52**(3), 505–519 (2005).
- ²¹J. Gellermann, M. Weihrauch, C. H. Cho, W. Wlodarczyk, H. Föhling, R. Felix, V. Budach, M. Weiser, J. Nadobny, and P. Wust, “Comparison of MR-thermography and planning calculations in phantoms,” *Med. Phys.* **33**(10), 3912–3920 (2006).
- ²²J. Lunze, *Regelungstechnik Band 2 – Mehrgrößensysteme, digitale Regelung.*, 2nd ed. (Springer Verlag, 2001).
- ²³J. Lunze, *Regelungstechnik Band 1 – Systemtheoretische Grundlagen, Analyse und Entwurf einschleifiger Regelungen.*, 3rd ed. (Springer Verlag, 2001).
- ²⁴E. Hutchinson, M. Dahleh, and K. Hynynen, “The feasibility of MRI feedback control for intracavitary phased array hyperthermia treatments,” *Int. J. Hyperthermia* **14**(1), 39–56 (1998).
- ²⁵D. Arora, M. Skliar, and R. B. Roemer, “Model-predictive control of hyperthermia treatments,” *IEEE Trans. Biomed. Eng.* **49**(7), 629–639 (2002).
- ²⁶P. Wust, J. Gellermann, M. Seebass, H. Föhling, W. Wlodarczyk, J. Nadobny, B. Rau, B. Hildebrandt, A. Oppelt, and R. Felix, “Teilkörperhyperthermie mit einem

- Radiofrequenz-Multiantennen-Applikator unter on-line Kontrolle in einem 1,5 T MR-Tomographen,” *Fortschr Röntgenstr* **176**, 363-374 (2004).
- ²⁷J. Gellermann, W. Wlodarczyk, A. Feussner, H. Föhling, J. Nadobny, B. Hildebrandt, R. Felix, and P. Wust, “Methods and potentials of magnetic resonance imaging for monitoring radiofrequency hyperthermia in a hybrid system,” *Int. J. Hyperthermia* **21**(6), 497–513 (2005).
- ²⁸M. E. Kowalski, B. Behnia, A. G. Webb, and J.-M. Jin, “Optimization of electromagnetic phased-arrays for hyperthermia via magnetic resonance temperature estimation,” *IEEE Trans. Biomed. Eng.* **49**(11), 1229–1241 (2002).
- ²⁹M. E. Kowalski and J. M. Jin, “A temperature-based feedback control system for electromagnetic phased-array hyperthermia: theory and simulation,” *Phys. Med. Biol.* **48**(5), 633–651 (2003).
- ³⁰S. K. Das, E. A. Jones, and T. V. Samulski, “A method of MRI-based thermal modelling for a RF phased array,” *Int. J. Hyperthermia* **17**(6), 465–482 (2001).
- ³¹T. Köhler, P. Maass, P. Wust, and M. Seebass, “A fast algorithm to find optimal controls of multiantenna applicators in regional hyperthermia,” *Phys. Med. Biol.* **46**(9), 2503–2514 (2001).
- ³²P. Wust, H. Stahl, J. Löffel, M. Seebass, H. Riess, and R. Felix, “Clinical, physiological and anatomical determinants for radiofrequency hyperthermia,” *Int. J. Hyperthermia* **11**(2), 151–167 (1995).
- ³³W. Tilly, P. Wust, B. Rau, C. Harder, J. Gellermann, P. Schlag, V. Budach, and R. Felix, “Temperature data and specific absorption rates in pelvic tumours: predictive factors and correlations,” *Int. J. Hyperthermia* **17**(2), 172–188 (2001).
- ³⁴P. Deuffhard and A. Hohmann, *Numerische Mathematik I.*, 3rd ed. (Walter de Gruyter, Berlin, 2002).
- ³⁵P. Wust, R. Beck, J. Berger, H. Föhling, M. Seebass, W. Wlodarczyk, W. Hoffmann, and J. Nadobny, “Electric field distributions in a phased-array applicator with 12 channels: measurements and numerical simulations,” *Med. Phys.* **27**(11), 2565–2579 (2000).
- ³⁶P. Wust, H. Föhling, W. Wlodarczyk, M. Seebass, J. Gellermann, P. Deuffhard, and J. Nadobny, “Antenna arrays in the SIGMA-eye applicator: interactions and transforming networks,” *Med. Phys.* **28**(8), 1793–1805 (2001).
- ³⁷J. Gellermann, W. Wlodarczyk, B. Hildebrandt, H. Ganter, A. Nicolau, B. Rau, W. Tilly, H. Föhling, J. Nadobny, R. Felix, and P. Wust, “Noninvasive magnetic resonance thermography of recurrent rectal carcinoma in a 1.5 Tesla hybrid system,” *Cancer Res.* **65**(13), 5872–5880 (2005).
- ³⁸J. D. Poorter, C. D. Wagter, Y. D. Deene, C. Thomsen, F. Ståhlberg, and E. Achten, “Noninvasive MRI thermometry with the proton resonance frequency (PRF) method: in vivo results in human muscle,” *Magn. Reson. Med.* **33**(1), 74–81 (1995).
- ³⁹D. Stalling, M. Westerhoff, and H.-C. Hege, “Amira: A highly interactive system for visual data analysis,” in *The Visualization Handbook*, edited by C. D. Hansen and C. R. Johnson, chapter 38, pages 749–767, Elsevier, 2005.

- ⁴⁰G. Sreenivasa, J. Gellermann, B. Rau, J. Nadobny, P. Schlag, P. Deuffhard, R. Felix, and P. Wust, “Clinical use of the hyperthermia treatment planning system HyperPlan to predict effectiveness and toxicity,” *Int. J. Radiat. Oncol. Biol. Phys.* **55**(2), 407–419 (2003).
- ⁴¹J. Nadobny, D. Sullivan, P. Wust, M. Seebass, P. Deuffhard, and R. Felix, “A high-resolution interpolation at arbitrary interfaces for the FDTD method,” *IEEE Trans. Microwave Theory Tech.* **46**(11), 1759–1766 (1998).